

(*掲載記事題目及び掲載頁は変更になる場合があります。*)

Fundamentals of High Temperature Processes
Interfacial phenomena during wetting of graphite/alumina mixtures by liquid iron

 L.ZHAO *et al.*

Carbon and alumina are important components in refractories used in the steel industry. High temperature interactions of the refractory materials with liquid metal are crucial in dictating the chemical reactions occurring at the interface, this will control the life of refractory and also the metal quality. Although, the high temperature interactions of graphite and alumina (each separately) with liquid iron have been investigated, fundamental understanding of high temperature interactions of graphite/alumina mixtures with liquid iron is far from complete. This is the focus of the present study. This study reports on the interfacial phenomena during wetting of C/Al₂O₃ mixtures by liquid iron.

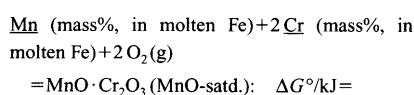
On a graphite substrate, the carbon content of liquid iron was 5.62% at 1600°C. This is the saturation concentration of carbon under the experimental condition. During the graphite/iron interactions, the contact angle changed from 64° at the initial state, to 38° at the final state. There is good wettability between iron and graphite. However, adding different amounts of alumina in the graphite substrate caused the contact angle to increase. When the alumina in the substrate increased from 16.7 to 23.1%, the contact angle demonstrated a sharp change from good wetting to almost non-wetting. The underlying phenomena dictating these changes are discussed. The carbon transfer reaction occurring at the solid/iron interface plays a key role in governing the wetting at the interface. At high rates of carbon dissolution, good wetting is observed. However, when the alumina in the substrate increased from 16.7 to 23.1%, the carbon content of iron shows a sharp decrease, and poor wetting is observed. These results, for the first time, bring out the interdependence of wetting and carbon dissolution during the high temperature interactions of graphite/alumina materials with liquid iron.

 (cf. *ISIJ Int.*, 43 (2003), 1)

Standard Gibbs free energy of formation of MnO-saturated MnO·Cr₂O₃ solid solution at 1873 K

 M.TANAHASHI *et al.*

The standard Gibbs free energy of formation of MnO-saturated MnO·Cr₂O₃ solid solution (stoichiometric MnO·Cr₂O₃), which is one of important thermodynamic properties of the MnO-SiO₂-CrO_x inclusion system to clarify the equilibrium relation among molten stainless steel and the inclusions formed during the stainless steel Si-deoxidation process, was determined at 1873 K. By equilibrating molten iron or copper with MnO-saturated MnO·Cr₂O₃ crucible under controlled oxygen partial pressure, P_{O_2} , the standard Gibbs free energy changes of the following reactions at 1873 K were determined to be:



$$-755 \pm 4 (P_{O_2} = \times 10^{-6} - 6 \times 10^{-5} \text{ Pa})$$

$$\underline{Mn} \text{ (mass\%, in molten Cu)} + 2 \underline{Cr} \text{ (mass\%, in molten Cu)} + 2 O_2 \text{ (g)}$$

$$\begin{aligned} = MnO \cdot Cr_2O_3 \text{ (MnO-satd.)}; \quad \Delta G^\circ/kJ = \\ -807 \pm 7 (P_{O_2} = 3 \times 10^{-5} - 1.5 \times 10^{-4} \text{ Pa}) \end{aligned}$$

$$Mn \text{ (l)} + 2 \text{ Cr (s)} + 2 O_2 \text{ (g)} = MnO \cdot Cr_2O_3 \text{ (MnO-satd.)};$$

$$\Delta G_{f, MnO \cdot Cr_2O_3}^\circ / kJ \cdot mol^{-1} = -958 \pm 8 (P_{O_2} = 2 \times 10^{-6} - 1.5 \times 10^{-4} \text{ Pa})$$

The values of ΔG° and $\Delta G_{f, MnO \cdot Cr_2O_3}^\circ$ are independent of the oxygen partial pressure within the P_{O_2} range in the present study.

 (cf. *ISIJ Int.*, 43 (2003), 7)

Interfacial kinetics of nitrogen with molten iron containing sulfur

 J.LEE *et al.*

The effect of sulfur on the interfacial reaction rates of nitrogen dissolution into molten iron has been investigated at 1823 K using an isotope-exchange technique. In addition, surface activities of the vacant sites and the sites occupied by sulfur have been proposed to predict the interfacial reaction rates and to clarify the rate-determining step of nitrogen dissolution into molten iron using the sulfur adsorption that had been obtained in our previous study. It was found that the experimental results were in good accordance with the predicted values for adsorbed N₂ dissociation control rather than those for N₂ adsorption control in the low sulfur activity region, yielding that the dissociation of nitrogen molecule into atoms at the surface is the rate-determining step of the interfacial reaction of nitrogen dissolution into molten iron. However, with increasing sulfur content, the experimental results showed higher values than the predicted ones assuming that reactions only occur at vacant sites. In the high sulfur content region, it was considered that reactions at occupied sites might occur. Accordingly, the total interfacial reaction rate constant (mol/cm²sec atm) of nitrogen dissolution could be expressed as $k = 6.2 \times 10^{-5} a_s^2 + 4.0 \times 10^{-7} a_s^2 + 7.0 \times 10^{-6} a_s a_\theta$.

 (cf. *ISIJ Int.*, 43 (2003), 14)

Ironmaking
Characterization of preparing cold bonded pellets for direct reduction using an organic binder

 G.QIU *et al.*

This paper involves the preparation technologies of cold bonded pellets for direct reduction using an organic binder-Funa. Investigation shows that the binder possesses excellent adhesive abilities to iron ore concentrates and is the key to the preparation of cold bonded pellets. Pretreatment on the binder-bearing iron concentrates prior to balling operation is essential to the maximization of adhesion of the binder to ore particles. Roll drum milling was found to be an effective method for the purpose. Investigation also shows iron ore concentrate containing the organic binder has a lower balling kinetics than bentonite concentrate due to the increased viscosity by

the binder. A balling time of 20 min is needed to ensure the pellet strength. It is found that the appropriate drying and hardening conditions for wet balls are 200–250°C of temperature and 0.8–1.0 m/s of airflow rate. TGA and DTA detection shows that the organic binder is thermally stable below 250°C in either neutral or oxidative atmosphere. Under above conditions, cold bonded pellets with a compressive strength of 250–300 N/Pellet, a drop strength of 7–10 times/1.0 m and a resistance to abrasion over 98% (+3 mm) have been attained from magnetite concentrates by using 1.5% of the organic binder. Tests show that the cold bonded pellets present a greater reduction rate and a higher iron grade of products than fired pellets made with bentonite as binder.

 (cf. *ISIJ Int.*, 43 (2003), 20)

The use of coated pellets in pptomising the blast furnace operation

 J.STERNELAND *et al.*

With the aim to improve the blast furnace process, coating of blast furnace pellets was investigated in laboratory scale as well as in the LKAB experimental blast furnace. Olivine, dolomite and quartzite respectively were applied as coating agents onto the regular LKAB olivine pellet MPBO. Testing of the coated pellets revealed the following: i) Dust generation was significantly decreased when using coated pellets in the blast furnace, ii) Sticking was prevented by the coating material. This was verified in different laboratory tests, as well as by studying probe samples from the blast furnace, and iii) Gas utilisation was higher for all coated pellets, with a lower variation, indicating a smoother blast furnace operation. Coating of pellets is considered as a significant improvement in optimising the blast furnace operation.

 (cf. *ISIJ Int.*, 43 (2003), 26)

A theoretical model for the contact phenomenon of coke particle accompanied by the compressive breakage at the contact plane

 H.YAMAOKA *et al.*

This study considers the mechanism of the breakage contact of coke particles. A theoretical model has been developed standing on the hypotheses as follows:

- (1) The breakage mode of coke particle is the surface compressive breakage.
- (2) The Hertzian stress distribution is induced on the contact plane of particle surface but the region with the Hertzian stress over than the compressive strength makes contact breakage and the stress on this region reduces to the value equal to the compressive strength.
- (3) The energy to be consumed during breakage contact is equal to the energy to be consumed for producing breakage fragments (fines) and is in proportion to the mass of fines.

On the basis of these hypotheses, the relationship between contact force and contact displacement was formulated and additionally, the breakage volume, the consumed energy, the restitution coefficient or the friction coefficient at normal, rotating and slip-

ping contact were expressed as a function of contact force and coke mechanical properties.

Particle dropping tests and simple shear tests were performed to check the authenticity of the breakage contact model and the impact forces measured at the particle dropping tests, the friction coefficient as well as the mass of generated fines at the simple shear tests were confirmed well agree with the values predicted by the model.

(cf. *ISIJ Int.*, 43 (2003), 36)

Development of a size degradation model of coke particles at the drum test and inside the blast furnace

H. YAMAOKA *et al.*

Experimental as well as theoretical studies were made on the basis of the breakage contact model to elucidate the breakage mechanism of cokes in the drum tests and the following equation to express the size distribution of cokes after breakage was obtained.

$$R(Dp, t) = \{1 - (Dp/Dp_s)^{3(E/M)(wt)}\} \\ \times \exp[-\{wt/(E/M)\}(Dp/Dp_{\max})^Y]$$

Here in the equation, $R(Dp, t)$ is the size distribution function at time t in the cumulative oversize of Dp . The key w means the specific work rate cokes suffer from the breakage system. Dp_s is the size of sample and Dp_{\max} is the maximum size to breakage fragments. The key (E/M) means the specific energy loaded per unit mass of breakage fragment and is named apparent fines generation energy. The key Y is the size distribution index to characterize the size distribution profile of the breakage fragments. These two parameters dominate the breakage phenomena and their values are given as functions of the mechanical properties of sample coke and the mechanical load conditions of the concerned breakage system.

The equation was confirmed useful to predict the breakage phenomena throughout the experiments with using three kinds of drum machine.

(cf. *ISIJ Int.*, 43 (2003), 44)

Casting and Solidification

Hot cracking behavior of Fe-Ni alloys via direct observation

J.D. LEE

Hot cracking behavior of Fe-Ni alloys was investigated by using a high-speed camera to observe hot cracking in samples that were temperature-gradient heated and tensile deformed. The susceptibility to hot cracking was reliably evaluated based on critical strain and crack propagation length as functions of Ni content and cool side temperature. Grain size and shape in the brittle temperature region depended on liquid boundary migration due to solute diffusion within the liquid boundary under temperature gradient. High susceptibility to hot cracking of Fe-Ni alloys could be explained by the high sulfur segregation near the grain boundary and the large grain size within the solid/liquid coexisting region due to the rapid migration of the liquid boundary.

(cf. *ISIJ Int.*, 43 (2003), 54)

Prediction of density of chromium steels by using the relation obtained from sessile drop method and thermodynamic phase calculation data

H. MIZUKAMI *et al.*

The change in the density of chromium steels with phase at a temperature range from 1000 to 1973 K have been studied by a sessile drop profile method. Measurement of the density by a sessile drop profile method has to be carried out under heating conditions to avoid the influence of both undercooling and the shrinkage within the sample during solidification. The density of chromium steels were dependent on the phase but not chromium contents. The density in the liquid, δ and γ single phase, (liquid+ δ), (liquid+ γ), (δ + γ) coexisting states and (liquid+ δ + γ) coexisting state could be predicted using the experimental results.

(cf. *ISIJ Int.*, 43 (2003), 63)

Chemical and Physical Analysis

SIMS/XPS studies of surface layer formed in Fe-Si-Mn alloys by oxygen penetration

S. SUZUKI *et al.*

Secondary ion mass spectrometry (SIMS) and X-ray photoelectron spectroscopy (XPS) have been used for analyzing surface layers formed in Fe-Si-Mn alloys containing 1, 2, 3 and 4.5 mass% silicon, which were annealed in hydrogen and argon gases with a low partial pressure of oxygen. SIMS depth profiles showed that silicon in these alloys is reacted with oxygen penetrating into the bulk to form silicon oxides, and the characteristic distribution of silicon oxides is obtained in the surface layer, depending on the bulk silicon concentration. Manganese in the alloys was also found to be enriched to the outer side of the surface layer. On the other hand, XPS results showed that silicon and manganese are enriched on the top surface in these alloys, and the surface concentration of these elements depends on the bulk silicon concentration.

(cf. *ISIJ Int.*, 43 (2003), 71)

Forming Processing and Thermomechanical Treatment

Analysis of chatter in tandem cold rolling mills

Y. KIMURA *et al.*

This paper is concerned with chatter in tandem cold rolling mills, which has been recognised to have close relation with friction conditions in roll bites. However, the relation between rolling conditions and the stability of vibration has not been clearly understood. Therefore, an attempt is made to understand how the rolling conditions can be related with vibration phenomena, through numerical simulations.

Firstly, a theoretical model is constituted to simulate the vibrational behaviour of a five-stand continuous rolling mill, and the stability of the mill vibration is evaluated, introducing a disturbance to the static rolling conditions. The results of the calculation show that the vibration is greatly influenced by rolling speed and friction coefficient. With increase

in rolling speed, the mill vibration tends to be self-excited. Also, the results show that optimal range of friction coefficient exists in which the vibration is damped and the mill is stable against the disturbance.

Secondly, a simple self-excited vibration model is proposed and the stability index is proposed for further understanding of the phenomena. An analytical approach is made to predict the stability of the rolling process. With this model, it is shown that the rolling force and the delay of the response to the change in gap have a major effect on self-excited vibration. Also, the calculated optimal range of friction coefficient in the continuous rolling simulation can be explained by using the analytical model.

(cf. *ISIJ Int.*, 43 (2003), 77)

Welding and Joining

Weldbonding of stainless steel

P.K. GHOSH *et al.*

Lap joints of 1.0 mm thick austenitic stainless steel sheets were prepared by adhesive bonding, conventional resistance spot welding and weldbonding processes. The weldbonding was carried out by adhesive joining followed by resistance spot welding of two pieces and immediate curing at temperature of 120°C for 60 min. The same schedule of curing was also applied in preparation of adhesive joints of the sheets. Prior to joining, the faying surfaces of the two sheets were always polished with 400 grade emery paper. The thickness of adhesive layer resulting maximum shear-tensile load bearing capacity of the joint was optimised. The size of weld nugget, microstructures of the weld and HAZ and hardness of the nugget and HAZ, resulted from different welding parameters (current and time), in both the resistance spot welds and weldbonds were studied. The ultimate shear-tensile load bearing capacity of the resistance spot welds and weldbonds are also compared and correlated with the welding parameters. The fatigue properties of the resistance spot weld and weldbond, having maximum strength, were also tested. The fracture behaviour of all the three types of joints was studied under optical stereo microscope. The weldbonds prepared at optimum process parameters were found to have superior mechanical properties than those of the conventional resistance spot welds, especially under dynamic loading.

(cf. *ISIJ Int.*, 43 (2003), 85)

Surface Treatment and Corrosion

Steam oxidation resistance of Ni-Cr thermal spray coatings on 9Cr-1Mo Steel. Part 1: 80Ni-20Cr

T. SUNDARARAJAN *et al.*

The steam oxidation resistance of 80%Ni-20%Cr metallic coatings has been evaluated at four different steam temperatures in the range of 600-750°C. Substrate used for the study was 9Cr-1Mo type steel. The thermal spray coatings were carried out using two different processes, viz., atmospheric plasma spray (APS) and high velocity oxy fuel (HVOF) spray. Thickness of the coatings was about 40 and

60 μm respectively. The results show that the thick and dense HVOF coating showed a better steam oxidation resistance than the thin porous APS coatings. At prolonged aging (1000 h) the HVOF coating showed the best protection till the temperature range of 650°C. Beyond this temperature the presence of Fe_2O_3 was noticed at the coating surface. The reason for the protectiveness and failure at higher temperatures (above 650°C) are discussed in detail.

(cf. *ISIJ Int.*, **43** (2003), 95)

Steam oxidation resistance of Ni-Cr thermal spray coatings on 9Cr-1Mo Steel. Part 2: 50Ni-50Cr *T.SUNDARARAJAN et al.*

The present work is focused on the steam oxidation resistance of 50%Ni-50%Cr metallic coatings produced using atmospheric plasma spray (APS) and high velocity oxy fuel (HVOF) spray processes on 9Cr-1Mo type steel substrate. Thickness of the coatings obtained in the HVOF and APS processes were about 60 and 40 μm respectively. The steam oxidation resistance of the coatings was evaluated at four different temperatures viz., 600, 650, 700 and 750°C. The results showed that the thick and denser HVOF coating yielded a better steam oxidation resistance than the thin and porous APS coatings. At prolonged aging (1000 h), the HVOF coating showed the best protection in all tested steam temperatures. APS coating performed satisfactorily well till the 100 h of test duration. But, it started the scale initiation at the coating interface and incorporation of scales occurred at 1000 h of steam oxidation test. The reason for the protectiveness by HVOF coating and failure of APS coatings at prolonged aging are discussed in detail.

(cf. *ISIJ Int.*, **43** (2003), 104)

Mechanical Properties

Effects of W and Co on long-term creep strength of precipitation strengthened 15Cr ferritic heat resistant steels

Y.TODA et al.

Effects of W and Co on creep deformation and microstructure of fully annealed and precipitation strengthened 15Cr-3W ferritic steels at 923 and 973 K have been investigated, and the strengthening effects of W and Co in a long-term and high temperature service condition have been discussed. The effect of Co addition on the creep rupture strength of the steels is higher than that of the further addition of W in the short-term. However, the creep rupture life of the steel with 6 mass% W is longer than that of the steel with 3 mass% Co at the low stress condition of 50 MPa and 973 K. The increase in W content promotes the formation of intermetallic compounds such as χ phase. The addition of Co promotes the precipitation of fine M_{23}C_6 carbide within grains. The precipitation of carbide by Co addition is effective in improving the short-term creep strength for higher stress regions, whereas the formation of intermetallic compounds by W addition is more effective for lower stress and long-term creep life.

(cf. *ISIJ Int.*, **43** (2003), 112)

Effects of sintering conditions on the mechanical properties of metal injection molded 316L stainless steel

T.S.YOON et al.

In this work, tensile and fatigue properties of the metal injection molded 316L stainless steel were studied with the variation of sintering conditions. It was found that increasing sintering temperature and time resulted in a decrease in the porosity along

with an increase in the grain size. With decreasing porosity, tensile strength and elongation increased, while yield strength maintained constant, which was attributed to the balanced effects of decrease of porosity and grain coarsening. Tensile strength and elongation were found to be largely dependent on the porosity rather than on the grain size since the fracture occurred mainly by microvoid growth and coalescence. A quantitative analysis on the yield strength was tried by considering the classical Hall-Petch equation and mechanistic models for yield strength of porous materials. The fatigue crack growth resistance at low ΔK level was not largely decreased when the porosity was increased up to 8%, but was significantly decreased when the porosity was increased to 17%. It was discussed in relation to the intrinsic nature of pore morphology and the extrinsic nature of crack closure.

(cf. *ISIJ Int.*, **43** (2003), 119)

Fatigue strength of laser-processed hot work tool steel

Y.SUN et al.

Hot work tool steel with an application in the die-casting industry was chosen as the test material. Most of the failure of dies depends on the heat check due to cyclic thermal stress. So, the present work aims to find a repair method of the failed tool. The microstructure of the Nd:YAG laser-processed material is formed by dendritic structure hardened into martensite. The steel shows secondary hardening by tempering and fatigue softening by cyclic loading even at room temperature. The rotating bending fatigue strength can be recovered to almost initial value by heat treatment at secondary hardening temperature after laser-processing. As the result, it is concluded that the laser processing is suitable for the repair of heat check.

(cf. *ISIJ Int.*, **43** (2003), 127)